IEEE Robotics and Automation Letters (RA-L) paper, presented at ICRA 2024, Yokohama, Japan. Cite as RA-L paper.

Lightweight and Flexible Prosthetic Wrist with Shape Memory Alloy (SMA)-based Artificial Muscle and Elliptic Rolling Joint

Kyujin Hyeon, Chongyoung Chung, Jihyeong Ma, and Ki-Uk Kyung*, *Member, IEEE*

***Abstract*— This paper proposes a novel prosthetic wrist that emulates the anatomical structure of the human wrist, specifically the wrist bones and muscles responsible for wrist movements. To achieve a range of motion (ROM) and load-bearing capacity comparable to the human wrist joint, we designed an elliptic rolling joint as an artificial wrist joint, mimicking the two-row structures of carpal bones. The joint offers two degrees of freedom (DOFs) and can support high loads while also providing adequate ROM. In addition, we designed the artificial muscles using the properties of human muscles, such as moment arm and displacement, and implemented them as shape memory alloy (SMA) spring-based actuators. The resulting prosthetic wrist, incorporating the artificial joint and artificial muscles, is lightweight at only 50g and can perform functional ranges of motion, including 53° for flexion, 50° for extension, 40° for radial deviation, and 42° for ulnar deviation. The use of SMA spring actuators confers restoring force and flexibility to the prosthetic wrist, allowing it to withstand external disturbances. Furthermore, the proposed wrist can be utilized as a robotic wrist, affording two additional DOFs, the ability to lift loads more than 20 times its weight, and variable joint stiffness.**

Index Terms - Prosthetics and Exoskeletons, Biomimetics, Soft Robot Applications

I. Introduction

Robotic upper limb prosthetics have the potential to assist individuals who have undergone upper limb amputation, with an estimated 2.1 million such cases in the United States alone, and even more worldwide [1]. As over 60% of upper limb amputations are trans-carpal [2], the hands play a crucial role in performing activities of daily living (ADLs), resulting in the majority of research and commercial products being focused on robotic hands [2-6]. Prosthetic wrists are also vital components to enhance functionality and dexterity as they enable adjustment of hand posture [7]. Nevertheless, the availability of commercial prosthetic wrists remains limited, and their functionalities are restricted [7-9].

There are several requirements that need to be considered in designing prosthetic wrists. Firstly, a prosthetic wrist must possess at least two degrees of freedom (DOFs) since wrist motion involves two DOFs: flexion/extension (FE) and ulnar/radial deviation (UR) [7, 10]. In addition, a prosthetic wrist must be able to withstand heavy loads and move freely and smoothly. For that, it needs to achieve a balance between the competing requirements of strength, durability, range of motion (ROM), and flexibility [11, 12]. Given that the wrist is a distal part of the upper limb, it is crucial to maintain a lightweight design to minimize the load on other joints and improve energy efficiency [5].

There are several approaches to designing prosthetic wrists based on bio-inspiration to solve complex requirements [13, 14]. One proposed lightweight prosthetic wrists offered full DOFs and mimicked the carpal bone structures and ligament routing [13]. They achieved high ROM with pneumatic artificial muscles and nonlinear stiffness for low impedance and larger strength along the elongation of the ligaments. Other approaches also mimicked the structure of the carpal bone to enable effective swing [14]. They adjusted the design parameters to maximize ROM while minimizing the inter-distance deviation. Additionally, they used clutch and tendon-driven mechanisms for nonlinear changes in wrist stiffness.

The present study proposes a lightweight and flexible prosthetic wrist that features two DOFs. The artificial wrist joint was designed as an elliptical rolling joint, as illustrated in Fig. 1, and the artificial muscle was developed using a shape memory alloy (SMA) based actuator. The ellipsoidal-shaped joint is a commonly employed design for artificial wrists [15, 16]. However, due to the different radii of curvature at each point, it has a relatively small contact area. To address this limitation, we propose a wrist joint that

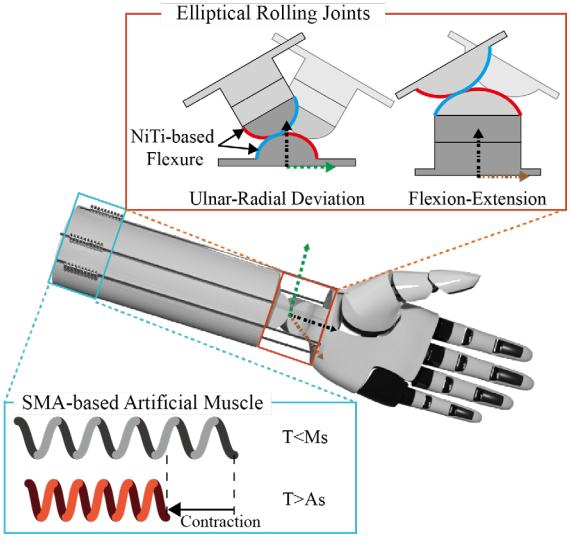

Figure 1. Conceptual design of the proposed prosthetic wrist

Manuscript received: May 25 2023; Revised: Aug. 17 2023; Accepted: Sep. 11 2023.

This paper was recommended for publication by Editor Pietro Valdastri upon evaluation of the Associate Editor and Reviewers' comments. This work was supported by the R&D program (No. 2022R1A2B5B02002074) of the National Research Foundation (NRF), Korea and the BK21 FOUR Program of the National Research Foundation Korea (NRF) grant funded by the Ministry of Education (MOE).

K. Hyeon, C. Chung, M, J. Ma, and K.U. Kyung are with the Korea Advanced Institute of Science and Technology, Daejeon, 34141 South Korea (e-mail: axz0502@kaist.ac.kr; cy.chung@kaist.ac.kr; wlgudak123@kaist.ac.kr; kyungku@kaist.ac.kr).

Digital Object Identifier (DOI): see top of this page.

IEEE Robotics and Automation Letters (RA-L) paper, presented at ICRA 2024, Yokohama, Japan. Cite as RA-L paper.

TABLE I. DIMENSION OF THE HUMAN WRIST

Parameter	*Value*
Thickness	40 mm
Height	30 mm
Width	60 mm

TABLE II. RANGE OF MOTION OF THE HUMAN WRIST

Wrist Motion	*Maximum*	*Functional*
Flexion	76°	54°
Extension	73°	48°
Radial Deviation	25°	22°
Ulnar Deviation	45°	38°

is based on an elliptic cylinder rolling joint, which reduces contact stress because of the larger radius of curvature within constrained dimensions [17]. Drawing upon the anatomy of carpal bones, we propose a two-row structured wrist, with each row featuring a different degree of freedom. To enhance the structural stability of the artificial joint, NiTi-based flexures, mimicking the ligament that attaches between bones to increase joint stability, are attached within the joint. These flexures form compliant rolling contact joints [18], preventing slippage between the rolling components of the joint.

To achieve a lightweight and flexible prosthetic wrist design, we selected an SMA-based actuator. SMA has been shown to possess the highest power density among soft actuators [19, 20]. When the temperature of SMA falls below its martensite start temperature (M_s), the elastic modulus of the SMA decreases, rendering it easily deformable. Conversely, when the SMA is heated above its austenite start temperature (A_s), its elastic modulus increases. The unique features of SMA actuators have garnered considerable interest as a potential substitute for conventional actuators in wearable technology [21-25]. In designing the SMA-based actuator, we considered the characteristics of human muscles that contribute to wrist movement. Subsequently, we integrated the artificial wrist and muscles to develop the prosthesis and evaluated its performance.

II. DESIGN PROCESS OF THE ARTIFICIAL WRIST JOINT

A. Human wrist and concept of the artificial wrist joint

Researchers have investigated its average dimensions in U.S. adults, and the findings are presented in Table I [7]. The human wrist has two DOFs, namely Flexion-Extension (FE) and Ulnar-Radial (UR). The ROMs for each of these movements can be divided into two categories: maximum ROMs, representing the extreme values for each DOF [7], and functional ROMs, which are the values necessary for performing ADLs in each DOF [7]. Both types of ROMs are detailed in Table II. The DOF movements of the wrist joint are a result of the rotational and gliding motion of each carpal bone, combined in various ways. Numerous models have been proposed to explain the movement of carpal bones, with the two-rowed structure being one of the most well-known, as depicted in Fig. 2 (a) [10, 16]. The two rows are ellipsoids connected serially and provide two degrees of freedom and a broad ROM. Furthermore, the significant motion of the proximal carpal row bones enables high flexibility in response to hand impact.

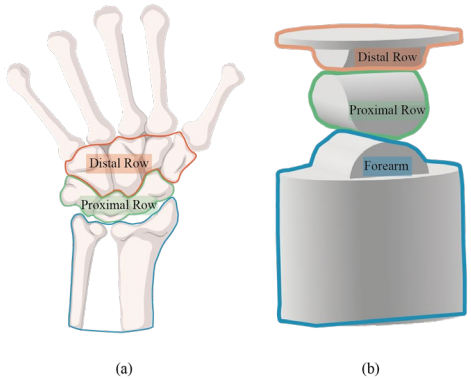

Figure 2. (a) Two-row structure of the carpal bones and (b) two-row structure of the artificial wrist joint

TABLE III. CHARACTERISTICS OF HUMAN WRIST MUSCLES

Muscles	*Function*	*Moment Arm (FE)*	*Moment Arm (UR)*	*PCSA (cm^2)*
FCR	Flexor/ Radial Deviator	15 mm	-10 mm	2.0
PL	Flexor	25 mm	0 mm	0.9
FCU	Flexor/ Ulnar Deviator	20 mm	15 mm	3.2
ECU	Extensor/ Ulnar Deviator	-10 mm	25 mm	3.8
ECRB	Extensor/ Radial Deviator	-15 mm	-15 mm	2.9
ECRL	Extensor/ Radial Deviator	-10 mm	-25 mm	2.1

Wrist motions are generated by six distinct muscles, namely the Flexor Carpi Radialis (FCR), Flexor Carpi Ulnaris (FCU), Extensor Carpi Radialis Longus (ECRL), Extensor Carpi Radialis Brevis (ECRB), Extensor Carpi Ulnaris (ECU), and Palmaris Longus (PL). The coordinated contraction of FCR, FCU, and PL with the extension of ECRL, ECRB, and ECU generates flexion of the wrist joint. Conversely, the reverse movement of each muscle compared to flexion motion causes extension of the wrist joint. Ulnar deviation is achieved by contracting FCU and ECU, whereas radial deviation is achieved by contracting FCR, ECRL, and ECRB. The moment arm, which governs the generation of torque in either the FE or UR direction, exhibits intermuscular variability. The average moment arm values for both directions of each muscle are documented in Table III. All of these muscles assume a fusiform shape, and their respective values of physical cross-sectional area (PCSA) are also presented in Table III.

In order to exploit the biomechanical properties of carpal bones, our approach involves designing an artificial wrist joint, which comprises two serially connected elliptic rolling joints. Rolling joints have been extensively employed owing to their numerous benefits, such as high flexibility, dexterity, reduced singularities, and enhanced workspace, particularly in hyper-redundant manipulators [26-30]. By adopting an ellipse shape for the rolling joints, a larger radius of curvature within constrained dimensions can be achieved, thus enabling greater load capacity while minimizing Hertz's contact stress [17]. Specifically, the rolling joint connecting the forearm bone and proximal carpal row facilitates flexion-extension motion, whereas the rolling joint between the proximal and

IEEE Robotics and Automation Letters (RA-L) paper, presented at ICRA 2024, Yokohama, Japan. Cite as RA-L paper.

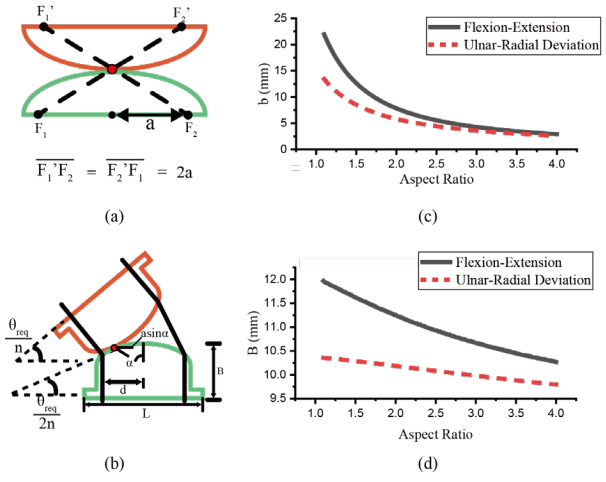

Figure 3. (a) The analogy of the kinematics of the elliptic rolling joint: the anti-parallelogram mechanism, (b) parameters of the elliptic rolling joint used in the design process, (c) results of the required minor axis radii as the aspect ratio of the ellipse change, and (d) results of the required minimum height of the elliptic rolling joint as the aspect ratio of the ellipse change.

distal carpal rows enables ulnar-radial deviation motion, as illustrated in Fig. 2 (b).

B. Artificial wrist joint design

When developing artificial wrist joints, it is essential to address various constraints. One of the primary concerns is dimensional constraints, which aim to replicate the size of a human wrist joint, as outlined in Table I. Additionally, the performance of the artificial wrist joint is closely tied to its ROM, which can be classified into two categories elaborated in Table II.

Since the wrist joint has an elliptical shape, the rolling joints can be considered an anti-parallelogram mechanism, as depicted in Fig. 3 (a) [17]. When an identical ellipse is rolled upon another ellipse, the distances of the two focal points are identical (as shown in Fig. 3 (a)), and the four focal points of the two ellipses form an anti-parallelogram. ($\overline{F_1F_2}, \overline{F_2F_1'}, \overline{F_1'F_2'}, \overline{F_2'F_1}$). Utilizing the anti-parallelogram mechanism, we resolved the kinematics of the rolling joints. The aspect ratio, which denotes the ratio between the minor axis and the major axis radius of the ellipse, was chosen as the design parameter for the rolling joint.

When designing the proposed rolling joint, it is essential to consider several constraints that are similar to those applied to conventional rolling joints [29, 30]. Although the shape of the proposed rolling joint differs, it must adhere to the design constraints of conventional rolling joints. This paper addresses a few of the key design constraints for the rolling joint. The first constraint concerns the correlation between the rotation angle range and the distance separating the tendon from the center of the rolling surface [30]. The constraint for conventional rolling joints can be expressed as

$$Rsin(\frac{\theta_{req}}{2n}) \leq d. \quad (1)$$

R is the radius of curvature of the rolling joint, θ_{req} is the rotation angle of the rolling joint, n is the number of the rolling joint, and d is the distance between the tendon and the center of the rolling joint. Failing to satisfy this condition will result in the generation of a torque in the opposite direction of the rolling, which thus impedes the rolling motion. This same constraint is applicable to the elliptical rolling joint. However, the rotation angle of the rolling joint (expressed as α in Fig. 3 (b)) and the rotation angle of the rolling surface (expressed as $\theta_{req}/2n$ in Fig. 3 (b)) are different from each other. Consequently, the constraint changes as

$$a \cdot sin\alpha \leq d. \quad (2)$$

a is the radius of the major axis of the elliptical rolling joint and α is the rotation angle of the rolling joint, as depicted in Fig. 3 (b).

In the design of the artificial wrist joint, the moment arm, d, corresponds to the length between the axis of the tendon and the axis of the rolling joint, which is dependent on the muscle involved in the motion. For the artificial wrist joint, we selected the minimum moment arm of these muscles as the value for d. The moment arm of each muscle is summarized in Table III. Specifically, the moment arm of the flexion/extension motion, $d_{f/e}$, and that of the ulnar/radial deviation motion, $d_{u/r}$, were set as 10 mm respectively. Moreover, the number of the rolling joints for flexion/extension motion, $n_{f/e}$, and that of ulnar/radial deviation motion, $n_{r/d}$, were both set to 1. The rotation angle of the rolling surface corresponding to the flexion/extension motion, $\theta_{req\_f/e}$, and ulnar/radial deviation motion, $\theta_{req\_u/r}$ were set to 75° and 45°, respectively. These values, presented in Table II, were chosen to design artificial joints based on the maximum ROM observed in the human wrist joint.

Under these conditions, we set the radius of the minor axis, b, as 1 and calculated $asin\alpha$ when $\theta_{req}/2n$ was achieved. Then we set the value of $d/asin\alpha$ as the scaling factor and calculated the required b as the aspect ratio increased. The results are shown in Fig. 3 (c). In both cases, the required b's were decreased as the aspect ratio increased.

Another design constraint considered in this study was the prevention of collision between adjacent rolling joints [30]. If the height of the rolling joint is insufficient, the adjacent joints may collide during rotation. The constraint for conventional rolling joints is expressed as

$$(B-R)\left(1+cos\left(\frac{\theta_{req}}{n}\right)\right)+2Rcos\left(\frac{\theta_{req}}{n}\right) \leq \frac{L}{2}sin\left(\frac{\theta_{req}}{n}\right). \quad (3)$$

B and L are the height and width of the rolling joint, respectively, and are shown in Fig. 3 (b). The same constraint is required for the elliptical rolling joint. However, the eccentricity of the ellipse changes (3) as follows.

TABLE IV. SELECTED DESIGN PARAMETERS

Parameters	*Value (mm)*
Radius of major axis for FE ($a_{f/e}$)	14.45
Radius of minor axis for FE ($b_{f/e}$)	12.63
Height for FE ($B_{f/e}$)	11.92
Radius of major axis for UR ($a_{u/r}$)	20.04
Radius of minor axis for UR ($b_{u/r}$)	14.40
Height for UR ($B_{u/r}$)	10.30

IEEE Robotics and Automation Letters (RA-L) paper, presented at ICRA 2024, Yokohama, Japan. Cite as RA-L paper.

TABLE V. SELECTED DESIGN PARAMETERS OF SMA SPRING

Muscles	A_s (°C)	M_s (°C)	n	N	d/D (mm/mm)	Required/Actual Displacement (mm/mm)
FCR	45.9	32.7	50	2	0.5/1.5	38/38
PL			60	1		45/45
FCU			60	3		45/45
ECU			65	4		47/49
ECRB			55	3		41/42
ECRL			65	2		47/49

$$(B - bcos\theta)(1 + cos(\frac{\theta_{req}}{n})) + asin(\frac{\theta_{req}}{n}) \leq \frac{L}{2} sin(\frac{\theta req}{n}). \quad (4)$$

For the design of the artificial wrist, the width of the rolling joint, denoted as L, is determined by the geometric constraints of the wrist, where $L_{f/e}$ represents the width of the rolling joint for flexion/extension and $L_{u/r,}$ represents the width of the rolling joint for ulnar/radial deviation. Specifically, $L_{f/e}$ should be equal to the thickness of the wrist, while $L_{u/r}$ should be equal to the width of the wrist, To ensure that there is no collision between adjacent rolling joints during rotation, a constraint is required, which has been previously discussed in [30]. Based on the results presented in Fig. 3 (c), the minimum height of the rolling joint, denoted as B, is calculated for different aspect ratios of the ellipse to prevent collision, as shown in Fig. 3 (d).

In order to achieve a wrist joint that is both compact and capable of bearing high loads, an optimization process was employed to select appropriate design parameters. Specifically, the height of the rolling joint was reduced to enhance compactness, while the curvature of the rolling joint was reduced to lower the contact stress and improve load-bearing capacity.

The determination of contact stress within the elliptical rolling joint follows the principles of Hertz contact theory [17]. According to this theory, the pressure distribution across the contact region conforms to a semielliptical prism, characterized by dimensions such as the major axis $2a$, minor axis $2b$, and width W [31]. The maximum pressure p_0 at the center of the distribution is given by

$$p_0 = 0.564\sqrt{\frac{P(2/r_{cur})}{L\Delta}} \quad (5)$$

where P is the normal force at the contact point, r_{cur} is the radius of the contact surfaces, and L is the width of the contact surface. Δ is a combined measure of Young's modulus, E, and Poisson's ratio, ν, for materials of rolling joints given by

$$\Delta = \frac{2(1-\nu^2)}{E} \quad (6).$$

Since the curvature of the rolling joint is not uniform for the ellipse, the average value of the curvature was utilized. A cost function was then defined as

$$C_i = B_i \cdot \frac{\int_0^{\theta req} \frac{1}{r_{cur}} d\theta}{\theta_{req}} (i = f/e \text{ or } u/r) \quad (7)$$

C is the defined cost function and r_{cur} represents the radius of the curvature for every point. The design parameters, the aspect ratio and height of the rolling joint, were then chosen to minimize the cost function. The optimization procedure including numerical integration was executed through manual computations using MATLAB. The outcomes are presented in Table IV.

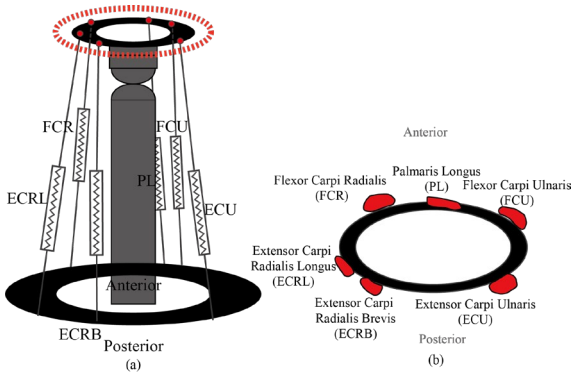

Figure 4. (a) The arrangements of the artificial muscles in (a) front and (b) top views.

C. Artificial Muscle Design

We developed a design for six artificial muscles that emulate the function of human muscles, whereby each muscle was fabricated using SMA springs. The SMA spring actuator is a linear actuator like human muscle and is activated as its temperature increases. Owing to its geometry, the coiled SMA spring actuator can generate an output deformation of up to 400% [32]. Several design parameters were considered for the artificial muscle. Firstly, SMA wire with a transition temperature from martensite to austenite (A_s) slightly higher than body temperature and a transition temperature from austenite to martensite (M_s) higher than room temperature was chosen [24]. The diameter of the SMA wire (d) was selected to be 0.5 mm and that of the SMA spring (D) to be 1.5 mm. Other parameters, such as the number of turns of each spring (n) and the number of springs (N), were chosen based on the properties of human muscles.

There are several ways to describe the force generated by muscles, one of them is using the *PCSA* [33]. The *PCSA* is the area of the cross-section of a muscle perpendicular to its muscle fibers not to its longitudinal axis. The force generated by the muscle can be described as

$$F_m = PCSA \cdot SF \cdot cos\phi \quad (8)$$

where F_m is the force generated by the muscle, SF is the specific force of the muscle, and ϕ is the pennation angle. Given that all muscles related to wrist motions are fusiform, the pennation angles are all 0. In the case of the force generated, the SMA spring can be described as

$$F_{sma} = N \cdot FS \quad (9)$$

where F_{sma} is the force generated by the muscle and FS is the force per spring. To ensure the proportional force ratio between each human muscle and artificial muscle, the number of springs in the artificial muscle was set according to the *PCSA* of the corresponding human muscle. The number of springs of each artificial muscle is presented in Table V.

To determine the appropriate number of turns (n) of each SMA spring, the required length change for each muscle was

IEEE Robotics and Automation Letters (RA-L) paper, presented at ICRA 2024, Yokohama, Japan. Cite as RA-L paper.

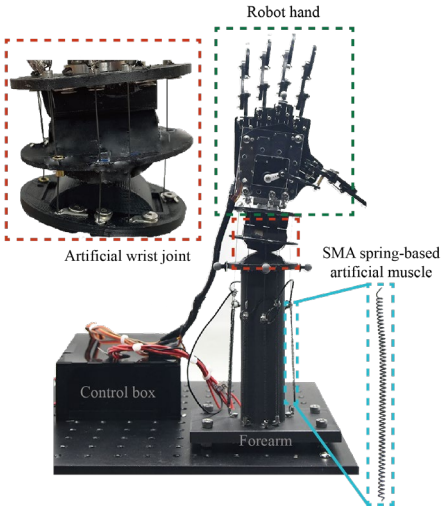

Figure 5. Integrated prototype with the artificial wrist joint, artificial muscle, forearm, robot hand, and control box

TABLE VI. MASS INFORMATION FOR EACH PART

Part	*Artificial Wrist Joint*	*Artificial Muscle*	*Forearm*	*Robot Hand*
Mass (g)	42.8	7.8	163	184.8

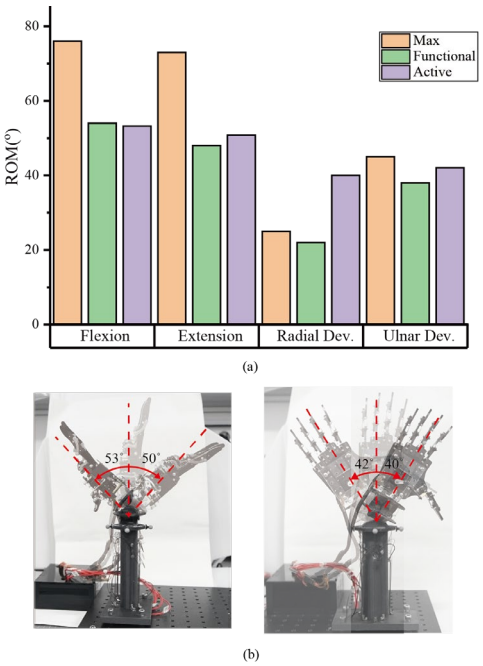

Figure 6. (a) The comparison with the max ROMs of the human wrist, the functional ROMs to perform ADLs of the human wrist, and the active ROMs of the prosthetic wrist and (b) the moment when the prosthetic wrist moves to its maximum ROMs in both directions, flexion/extension and radial/ulnar deviation.

calculated, rotating up to the maximum ROMs of the human wrist. For simplification, we had 3 assumptions: 1. The wrist joint was assumed to be a simple ball joint with a distance of 150 mm between the joint and the origin of muscles, and 20 mm between the joint and the insertion of muscles, 2. SMA spring can be deformed up to 50-350 % of its initial length (l_0), and 3. It was stretched 200% of its initial length when the wrist was in the neutral position.

Initially, the distance between the origin and insertion of the muscle is 170 mm when the joint angle assumes 0°. As the joint angle increases, this distance undergoes alteration, and its calculation is facilitated through the geometric construction of a triangle involving the insertion point, origin point, and ball joint. Under the assumption that each SMA spring contracts maximally (with a 50% stretch) from its neutral position, an inference is drawn that the wrist attains its maximum ROM. Notably, the extent of change in the artificial muscle's length between the neutral and contracted states corresponds to the variation in length between the muscle's origin and insertion. Consequently, this length alteration for the artificial muscle between its neutral and contracted states equates to 150% of the initial length of each spring (l_0). Hence, the determination of the number of turns (n) for each SMA spring is achieved by dividing the length disparity between the neutral and contracted states by 1.5 times the wire diameter (d). The specific design parameters chosen for each SMA spring actuator are thoughtfully collated within Table V for reference.

The SMA spring actuators were produced by adhering to the selected design parameters, following the process suggested in our previous works [22-24, 34-36]. They were affixed to predetermined anchor points according to the moment arms of the human wrist muscles. The attachment point of each artificial muscle was located in the forearm, while the insertion point was located in the hand. The arrangement of artificial muscles and joints in a parallel configuration between the hand and forearm can be seen in Fig. 4.

D. Prosthetic Wrist Design

The wrist joint prototype was constructed using onyx, a nylon-based thermoplastic polymer filled with micro carbon fiber which exhibited an elastic modulus of 2.4 GPa [37]. For the forearm prototype, carbon fiber-filled polyamide was utilized. Nitinol sheets with super-elasticity flexures were integrated into the design to facilitate smooth motion and prevent slippage between the rolling joints. These flexures served a dual purpose: they provided a restoring force to maintain the center alignment of the rolling joints and effectively prevented buckling or compression [18]. To ensure the desired shape memory properties, the Nitinol sheets were subjected to a temperature of 450 ℃ for one hour before being affixed to the rolling joints. Subsequently, they were assembled in an alternating sequence and deformed until both rolling joints aligned and seamlessly joined together [18]. Remarkably, the super-elasticity of the Nitinol sheets allowed them to recover their original shape even under high local strain. Emulating the function of ligaments in the human wrist, these flexures contributed to the increased structural stability of the joint system while effectively preventing sliding between the rolling joints.

Additionally, to minimize the friction force between the tendon and the artificial wrist joint, we incorporated tendon sheets made of polytetrafluoroethylene (PTFE) tubes, which have a low friction coefficient of 0.04 [38]. Finally, a robot hand and forearm were attached to the wrist joint. The prosthetic wrist, including the artificial wrist joint and muscle,

IEEE Robotics and Automation Letters (RA-L) paper, presented at ICRA 2024, Yokohama, Japan. Cite as RA-L paper.

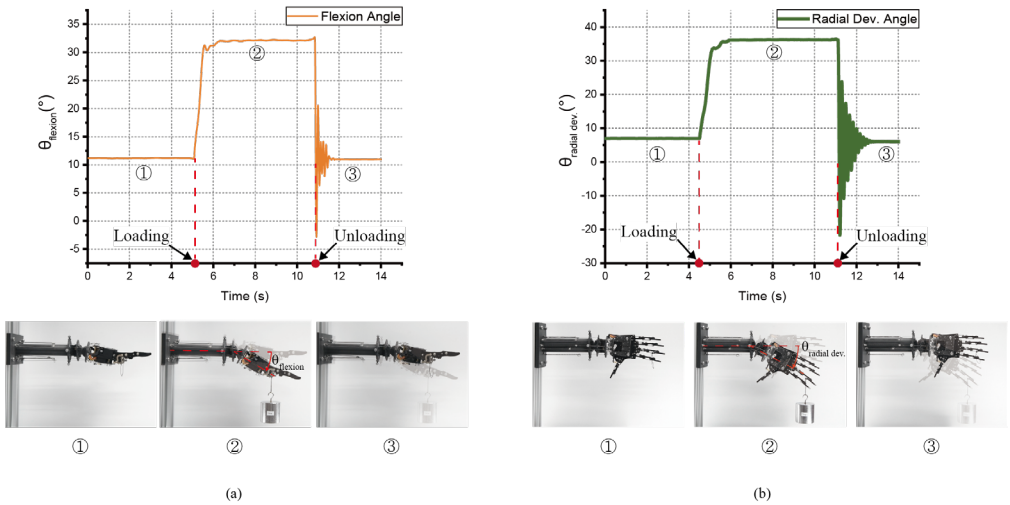

Figure 7. Location and image of the robot hand when a 1kg load is applied to the prosthetic wrist and suddenly unloading in (a) flexion/extension direction and (b) radial/ulnar direction.

weighed only 50 g and the total mass of the integrated prototype, including the forearm and robot hand, was approximately 400g. The individual masses of each component of the prototype are summarized in Table VI, and a picture of the integrated prototype is presented in Fig. 5.

III. Performance Evaluation

A. Active Range of Motion

To evaluate performance of the proposed prosthetic wrist, we undertook experiments to quantify the active ROM of the synthetic wrist. Specifically, we affixed four markers on the forearm and one on the hand to assess the ROM of the wrist joint utilizing a motion capture camera (V120 trio, OptiTrack). Subsequently, we applied a current of 1.5 A for ten seconds to the SMA springs implicated in each movement, followed by measuring the ROM of the wrist joint. The ROM achieved by the artificial wrist was then compared to the max ROMs and functional ROMs of the human wrist joint, and the results are presented in Fig. 6. It is noteworthy that the ROMs achieved by the prosthetic wrist, as a result of certain design assumptions made in the artificial muscle configuration, may not fully encompass the maximum ROMs of the human wrist, which constitutes the target of the prosthetic wrist's design. Nevertheless, the achieved active ROMs by the artificial wrist strongly correlated with the functional ROMs of the human wrist joint. This concurrence implies that the proposed device holds significant potential in facilitating the performance of ADLs for individuals with limb amputation.

B. Flexibility

The exceptional flexibility of the proposed prosthetic wrist is due to the restoring force exhibited by the SMA spring actuators and the supple nature of the rolling joint. To confirm the extent of this flexibility, we executed a trial whereby a 1kg load was attached to the robot hand and then abruptly disengaged. The results are shown in Fig. 7. Preceding the attachment of the 1kg load to the robot hand, a slight joint angle was elicited by the weight of the robot hand itself. Following the application of the 1kg load, the joint angle increased for both the flexion and radial deviation scenarios. Finally, upon removal of the 1kg load, a small oscillation ensued due to the flexibility of the SMA spring actuators, and the joint angle reverted to its pre-loading orientation.

The flexibility of the prosthetic wrist enhances robustness against impact or disturbance. The prosthetic wrist returns to its original position, even after being subjected to hammer impacts or deliberate shaking by hand, as demonstrated in Supplementary Video S3. Such a characteristic is pivotal for prosthetic wrists intended to interact with people or function in various everyday situations.

C. Robotic Applications

Although the proposed artificial wrist was primarily designed for use as a prosthesis, the potential applications of this wrist may extend to the realm of robotics. One promising avenue for robotics application involves affixing the wrist to a robot arm to confer two additional DOFs. The SMA spring actuator's high work density, which enables it to lift substantial loads, is a significant advantage. Fig. 8 (a) and (b) illustrate that the proposed wrist can successfully lift a 1kg load, which is over 100 times the mass of the artificial muscle, in both the FE and RU directions. In the proposed design, each artificial muscle was fashioned using SMA spring actuators that correspond to one-fold the PCSA of human muscles. By augmenting the number of SMA spring actuators employed in each artificial muscle, the payload capacity of the artificial wrist can be heightened, expanding the spectrum of robotic applications to which it may be suited.

Considering that the SMA spring actuators are thermally activated, it is noteworthy that their response time tends to be sluggish. As demonstrated in Fig. 8 (c) and (d), the time response of the SMA spring actuators is depicted upon the application of 1.5 A to each spring, corresponding to distinct directions. Augmenting the applied current can potentially decrease the response time, particularly during the heating phase; however, it is pivotal to improve the cooling performance through alternative strategies, such as the integration of an active cooling system. While the necessity

IEEE Robotics and Automation Letters (RA-L) paper, presented at ICRA 2024, Yokohama, Japan. Cite as RA-L paper.

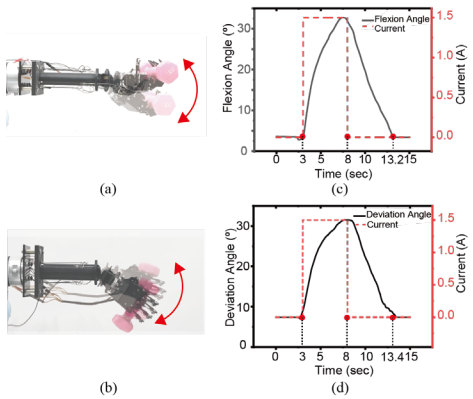

Figure 8. The moment when the prosthetic wrist lifts a 1kg load when it is attached to the robot arm in (a) flexion/extension and (b) ulnar/radial direction and the time response of the prosthetic wrist in (c) flexion/extension and (d) ulnar/radial direction.

for rapid response time may be relatively less crucial in the context of prosthetic wrist application, it assumes greater significance in the domain of robotics. In robotic applications, there exists a demand for heightened actuator response to effectively support desired functionalities.

Another potential robotic application that can be pursued leverages the controllability of joint stiffness exhibited by the proposed artificial wrist. The joint stiffness of the artificial wrist can be modulated by manipulating the temperature of the SMA spring actuators. In Fig. 9, an experiment is depicted to assess the capability of modulating joint stiffness in the prosthetic wrist. The evaluation involves the application of various loads—1 kg, 1.5 kg, and 2 kg—to the wrist for each DOF, with subsequent measurement of joint angles. The experimentation encompasses three distinct scenarios for each DOF: low stiffness (characterized by the absence of current, 0 A), medium stiffness (achieved through 0.75 A of current), and high stiffness (realized through 1.5 A of current). The outcomes reveal a significant capacity to alter stiffness, with the high stiffness condition exhibiting more than tenfold stiffness compared to the low stiffness scenario. However, it is notable that with an increase in joint angle, the stiffness diminishes due to the phase transition in the SMA actuators, initiated by the application of stress.

Fig. 10 depicts an experiment involving the use of a robot arm to smash an egg using a hammer with characteristics of variable joint stiffness. When the SMA spring actuators were not heated, the wrist joint exhibited insufficient stiffness to break the egg, and the wrist rotated in the radial direction. By contrast, when the SMA spring actuators were heated, the wrist joint displayed adequate stiffness to fracture the egg. This concept of modulating joint stiffness to match the task at hand is analogous to the human wrist, where higher joint stiffness is required to generate impact, whereas lower joint stiffness is employed to protect the body by increasing flexibility. Similarly, the proposed artificial wrist can offer variable joint stiffness to facilitate diverse applications.

IV. Conclusion and Future Works

We presented a novel design for a prosthetic wrist that utilizes an elliptic rolling joint and artificial muscles to achieve two DOFs, namely flexion-extension and radial-ulnar

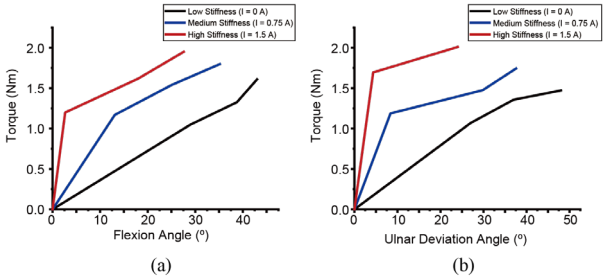

Figure 9. Modulating of the joint stiffness in (a) flexion/extension and (b) ulnar/radial direction by applying different amount of current.

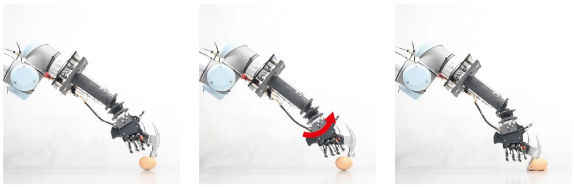

Figure 10. (a) The moment right before hitting the egg, (c) the moment right after hitting the egg with the flexible wrist joint, and (d) the moment right after hit the egg with stiff wrist joint.

deviation. The elliptic rolling joint was designed to allow for a ROM that is comparable to that of the human wrist joint with minimal contact stress and increased load-bearing capacity. The artificial muscles were constructed using SMA spring actuators that closely mimic the characteristics of the human wrist muscles.

The proposed prosthetic wrist demonstrates ROMs of 53° for flexion, 50° for extension, 40° for radial deviation, and 42° for ulnar deviation, which are comparable to the functional ROMs of the human wrist joint Moreover, the inherent spring-like configuration of the actuators imparts several advantageous characteristics. Notably, these actuators inherently generate restoring forces, resulting in exceptional flexibility, seamless return to the neutral state, and gravity compensation—achieved without any reliance on external energy inputs. Furthermore, the remarkable work density inherent to SMA equips the system with the dual benefits of being both lightweight and potent. This high work density attribute empowers direct attachment of the actuator to the joint, thus effectively curbing any potential loss of force or energy during transmission from the actuators. Beyond these benefits, the interplay of high work density and controllable stiffness in the SMA spring actuators broadens the applicability of the proposed wrist. Notably, this technology not only holds promise for prosthetic applications but also opens avenues for deployment in robotic wrists.

However, several issues need to be addressed in the future to further improve the performance of the proposed wrist. Although we have successfully demonstrated the concept of the wrist based on the SMA spring actuators, the response time of these actuators needs to be improved for practical use. To address this issue, various approaches have been proposed, such as integrating the SMA actuator with a coolant circulation system to improve the cooling rate and achieve an actuation frequency of 0.5 Hz[22, 23, 34, 35]. We plan to modify these structures to make them appropriate for the prosthetic wrist and further improve their response time in our future work.

IEEE Robotics and Automation Letters (RA-L) paper, presented at ICRA 2024, Yokohama, Japan. Cite as RA-L paper.

Furthermore, the envisaged wrist prosthesis incorporates a surplus of muscles compared to the available DOFs, thus resulting in redundant muscles. This surplus of muscles contributes to the complexity of the system; however, it is accompanied by a range of potential benefits, such as enhanced precision in control [39]. Nevertheless, during the design phase of the prosthetic wrist and the subsequent determination of the optimal number of actuators, there are constraints that necessitate consideration. In our future work, we intend to address this by developing a prosthetic wrist design that boasts an optimally balanced number of muscles.

REFERENCES

[1] K. Ziegler-Graham, E. J. Mackenzie, P. L. Ephraim, T. G. Travison, and R. Brookmeyer, "Estimating the Prevalence of Limb Loss in the United States: 2005 to 2050," *Arch. Phys. Med. Rehabil.,* vol. 89, no. 3, pp. 422-429, 2008.

[2] F. Cordella *et al.*, "Literature review on needs of upper limb prosthesis users," *Front. Neurosci.,* vol. 10, p. 209, 2016.

[3] J. T. Belter, J. L. Segil, and B. SM, "Mechanical design and performance specifications of anthropomorphic prosthetic hands: a review," *J. Rehabil. Res. Dev.,* vol. 50, no. 5, p. 599, 2013.

[4] R. Damerla, Y. Qiu, T. M. Sun, and S. Awtar, "A Review of the Performance of Extrinsically Powered Prosthetic Hands," *IEEE Trans. Med. Robot. Bionics,* vol. 3, no. 3, pp. 640-660, 2021.

[5] F. Montagnani, M. Controzzi, and C. Cipriani, "Is it Finger or Wrist Dexterity That is Missing in Current Hand Prostheses?," *IEEE Trans. Neural Syst. Rehab. Eng.,* vol. 23, no. 4, pp. 600-609, 2015.

[6] V. Mendez, F. Iberite, S. Shokur, and S. Micera, "Current Solutions and Future Trends for Robotic Prosthetic Hands," *Annu. Rev. Control Robot. Auton. Syst.,* vol. 4, no. 1, pp. 595-627, 2021.

[7] R. Damerla *et al.*, "Design and Testing of a Novel, High-Performance Two DoF Prosthetic Wrist," *IEEE Trans. Med. Robot. Bionics,* vol. 4, no. 2, pp. 502-519, 2022.

[8] N. M. Bajaj, A. J. Spiers, and A. M. Dollar, "State of the art in prosthetic wrists: Commercial and research devices," *Proc. 2015 IEEE International Conference on Rehabilitation Robotics (ICORR)*, Singapore, 2015: IEEE.

[9] OttoBock. Available: http://www.ottobock.com (accessed. Aug. 2023)

[10] J. Eschweiler *et al.*, "Anatomy, Biomechanics, and Loads of the Wrist Joint," *Life,* vol. 12, no. 2, p. 188, 2022.

[11] G. Lee, G. Y. Hong, and Y. Choi, "Tendon-Driven Compliant Prosthetic Wrist Consisting of Three Rows Based on the Concept of Tensegrity Structure," *IEEE Robot. Autom. Lett.,* vol. 6, no. 2, pp. 3956-3963, 2021.

[12] E. A. Biddiss and T. T. Chau, "Upper limb prosthesis use and abandonment: a survey of the last 25 years," *Prosthet. Orthotics Int.,* vol. 31, no. 3, pp. 236-257, 2007.

[13] N. Kim, S. Yun, and D. Shin, "A Bioinspired Lightweight Wrist for High-DoF Robotic Prosthetic Arms," *IEEE/ASME Trans. Mechatron.,* vol. 24, no. 6, pp. 2674-2683, 2019.

[14] M. H. Chang *et al.*, "Anthropomorphic Prosthetic Hand Inspired by Efficient Swing Mechanics for Sports Activities," *IEEE/ASME Trans. Mechatron.,* vol. 27, no. 2, pp. 1196-1207, 2022.

[15] A. Maciel, L. P. Nedel, and C. D. S. Freitas, "Anatomy-based joint models for virtual human skeletons," *Proc. Proceedings of Computer Animation 2002 (CA 2002)*, 2002: IEEE, pp. 220-224.

[16] O. Lewis, R. Hamshere, and T. Bucknill, "The anatomy of the wrist joint," *J. Anat.,* vol. 106, no. 3, pp. 539-552, 1970.

[17] J. R. Montierth, R. H. Todd, and L. L. Howell, "Analysis of elliptical rolling contact joints in compression," *J. Mech. Des.,* vol. 133, no. 3, p. 031001, 2011.

[18] L. A. Shaw, S. Chizari, M. Dotson, Y. Song, and J. B. Hopkins, "Compliant rolling-contact architected materials for shape reconfigurability," *Nat. Commun.,* vol. 9, no. 1, 2018.

[19] J. M. Jani, M. Leary, A. Subic, and M. A. Gibson, "A review of shape memory alloy research, applications and opportunities," *Mater. Des.,* vol. 56, pp. 1078-1113, 2014.

[20] J. Zhang *et al.*, "Robotic artificial muscles: Current progress and future perspectives," *IEEE Trans. Robot.,* vol. 35, no. 3, pp. 761-781, 2019.

[21] S. J. Park and C. H. Park, "Suit-type wearable robot powered by shape-memory-alloy-based fabric muscle," *Sci. Rep.,* vol. 9, no. 1, pp. 1-8, 2019.

[22] J. Jeong, I. B. Yasir, J. Han, C. H. Park, S.-K. Bok, and K.-U. Kyung, "Design of shape memory alloy-based soft wearable robot for assisting wrist motion," *Appl. Sci.,* vol. 9, no. 19, p. 4025, 2019.

[23] J. Jeong *et al.*, "Soft wearable robot with shape memory alloy (SMA)-based artificial muscle for assisting with elbow flexion and forearm supination/pronation," *IEEE Robot. Autom. Lett.,* vol. 7, no. 3, pp. 6028-6035, 2022.

[24] K. Hyeon, J. Jeong, C. Chung, M. Cho, S. Hussain, and K.-U. Kyung, "Design of a Wearable Mechanism With Shape Memory Alloy (SMA)-Based Artificial Muscle for Assisting With Shoulder Abduction," *IEEE Robot. Autom. Lett.,* vol. 7, no. 4, pp. 10635-10642, 2022.

[25] S. J. Park, K. Choi, H. Rodrigue, and C. H. Park, "Soft Exosuit Based on Fabric Muscle for Upper Limb Assistance," *IEEE/ASME Trans. Mechatron.,* 2022.

[26] H. Kim, J. M. You, M. Hwang, K.-U. Kyung, and D.-S. Kwon, "Sigmoidal Auxiliary Tendon-Driven Mechanism Reinforcing Structural Stiffness of Hyper-Redundant Manipulator for Endoscopic Surgery," *Soft Robot.,* 2022.

[27] J. Kim, S.-i. Kwon, Y. Moon, and K. Kim, "Cable-movable rolling joint to expand workspace under high external load in a hyper-redundant manipulator," *IEEE/ASME Trans. Mechatron.,* vol. 27, no. 1, pp. 501-512, 2021.

[28] Y.-J. Kim, S. Cheng, S. Kim, and K. Iagnemma, "A stiffness-adjustable hyperredundant manipulator using a variable neutral-line mechanism for minimally invasive surgery," *IEEE Trans. Robot.,* vol. 30, no. 2, pp. 382-395, 2013.

[29] J.-w. Suh, K.-y. Kim, J.-w. Jeong, and J.-j. Lee, "Design considerations for a hyper-redundant pulleyless rolling joint with elastic fixtures," *IEEE/ASME Trans. Mechatron.,* vol. 20, no. 6, pp. 2841-2852, 2015.

[30] D.-H. Lee, M. Hwang, J. Kim, and D.-S. Kwon, "Payload optimization of surgical instruments with rolling joint mechanisms," *Proc. 2020 IEEE/RSJ International Conference on Intelligent Robots and Systems (IROS)*, Las Vegas, NV, USA, 2020: IEEE.

[31] R. C. Juvinall, *Engineering Considerations of Stress, Strain, and Strength*. McGraw-Hill College, New York, 1967.

[32] S.-M. An, J. Ryu, M. Cho, and K.-J. Cho, "Engineering design framework for a shape memory alloy coil spring actuator using a static two-state model," *Smart Mater. Struct.,* vol. 21, no. 5, p. 055009, 2012.

[33] C. N. Maganaris, V. Baltzopoulos, D. Ball, and A. J. Sargeant, "In vivo specific tension of human skeletal muscle," *J. Appl. Physiol.,* vol. 90, no. 3, pp. 865-872, 2001.

[34] J. Jeong *et al.*, "Wrist Assisting Soft Wearable Robot With Stretchable Coolant Vessel Integrated SMA Muscle," *IEEE/ASME Trans. Mechatron.,* vol. 27, no. 2, pp. 1046-1058, 2022.

[35] J. Jeong, C. Hoon Park, and K.-U. Kyung, "Modeling and Analysis of SMA Actuator Embedded in Stretchable Coolant Vascular Pursuing Artificial Muscles," 2020: IEEE.

[36] K. Hyeon and K.-U. Kyung, "New Phase Diagram for Low Hysteresis Response of a Coiled Shape Memory Alloy Actuator," *Smart Mater. Struct.,* 2023.

[37] Markforged. http://www.markforged.com/ (accessed. Aug. 2023)

[38] S. Biswas and K. Vijayan, "Friction and wear of PTFE—a review," *Wear,* vol. 158, no. 1-2, pp. 193-211, 1992.

[39] M. G. E. Schneiders, M. J. G. Van De Molengraft, and M. Steinbuch, "Benefits of over-actuation in motion systems," 2004: IEEE.